Supporting Information

Modulation of Nucleation and Crystallization in PbI_2 Films Promoting Preferential Perovskite Orientation Growth for Efficient Solar Cells

Wenlong Shao,[a,b] Haibing Wang,[a] Feihong Ye,[a] Cheng Wang,[a] Chen Wang,[a] Hongsen Cui,[a] Kailian Dong,[a] Yansong Ge,[a] Ti Wang,[a] Weijun Ke,[*a,b] Guojia Fang[*a,b]

a. Key Laboratory of Artificial Micro- and Nano-structures of Ministry of Education of China, School of Physics and Technology, Wuhan University, Wuhan 430072, China

E-mail: weijun.ke@whu.edu.cn (W. Ke); gjfang@whu.edu.cn (G. Fang)

b. Shenzhen Institute, Wuhan University, Shenzhen 518055, China

* Corresponding author

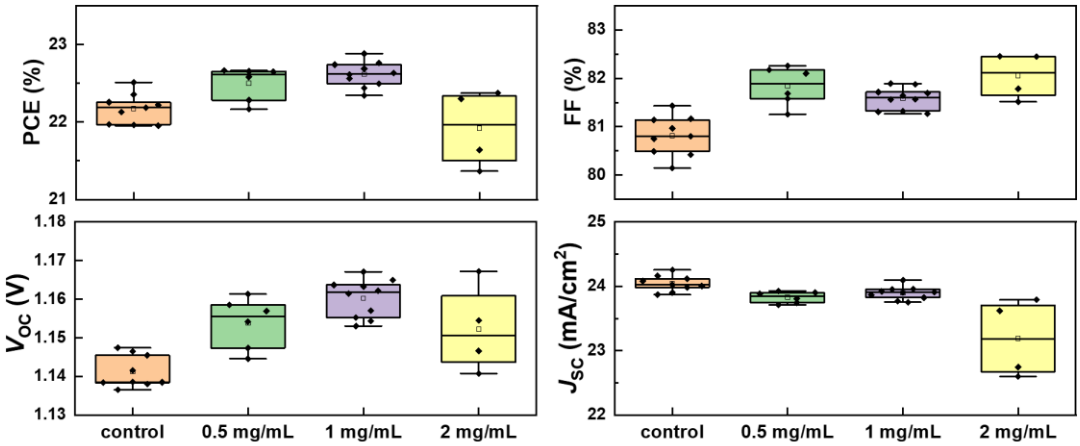

Figure S1. Statistical distribution of *J-V* parameters of devices containing 0 (control), 0.5, 1, and 2 mg/mL of PFAT.

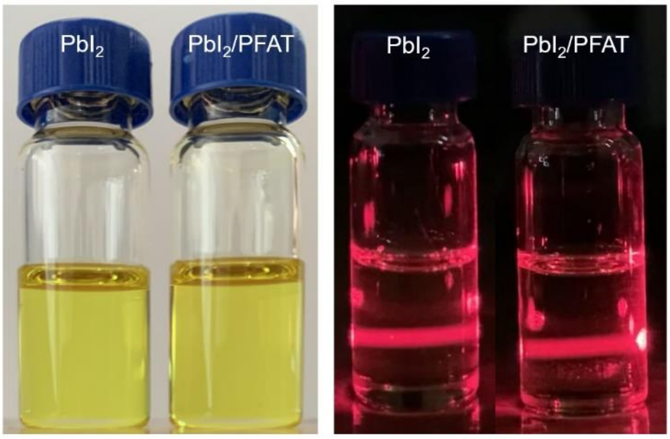

Figure S2. PbI_2 solutions in DMF/DMSO (950/50, volume) w/o and with PFAT, and the corresponding Tyndall effect optical images.

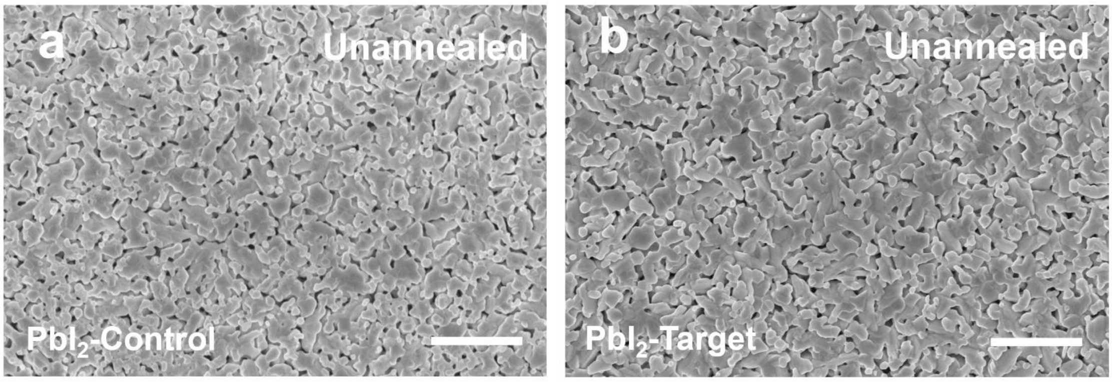

Figure S3. Top-view SEM images of the a) PbI_2-Control and b) PbI_2-Target unannealed films deposited on ITO/SnO_2 substrates. The scale bars represent 1μm.

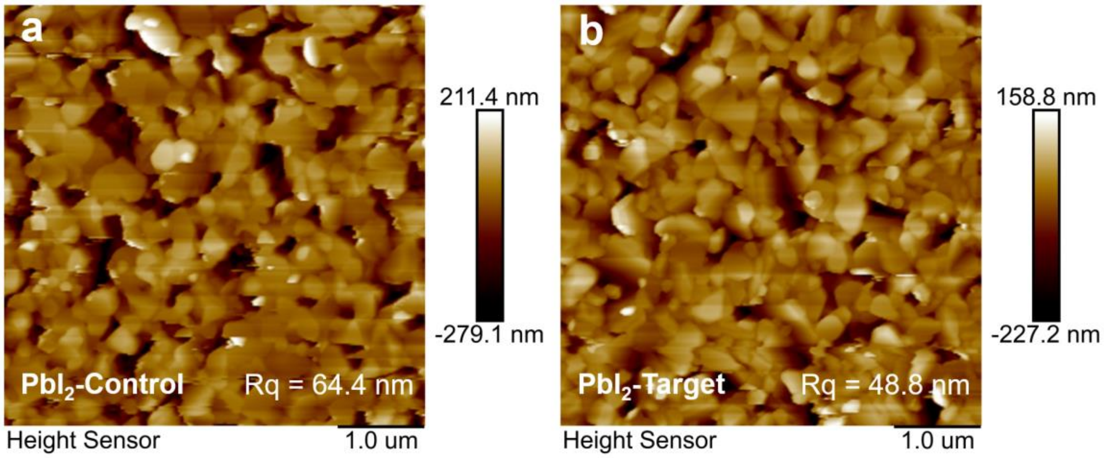

Figure S4. AFM 2D images of the a) PbI_2-Control and b) PbI_2-Target unannealed films deposited on ITO/SnO_2 substrates.

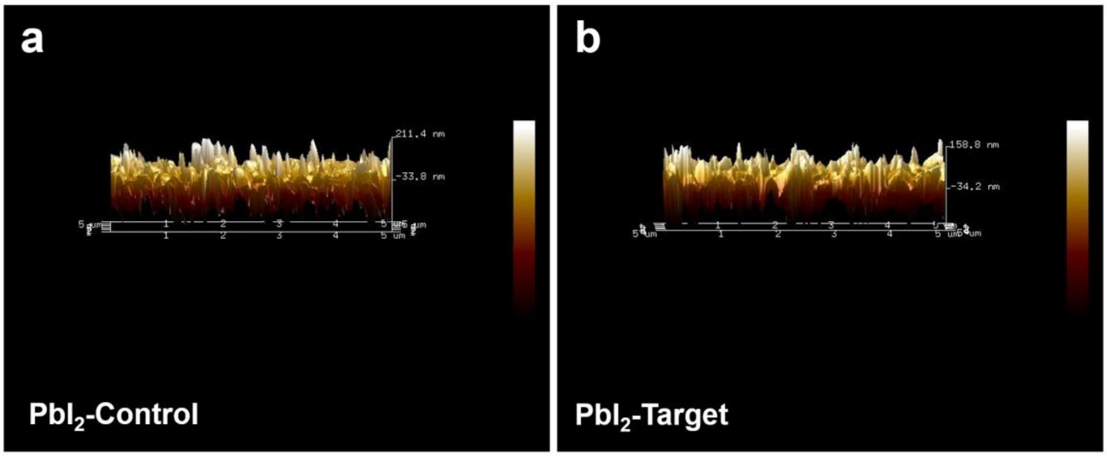

Figure S5. AFM 3D images of the a) PbI_2-Control and b) PbI_2-Target unannealed films deposited on ITO/SnO_2 substrates.

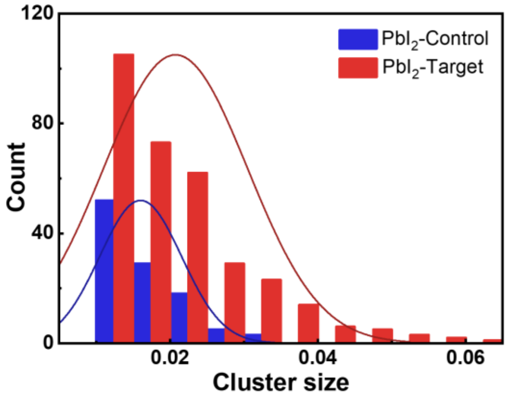

Figure S6. The statistics of cluster sizes in the PbI_2-Control and PbI_2-Target films from the top-view SEM images.

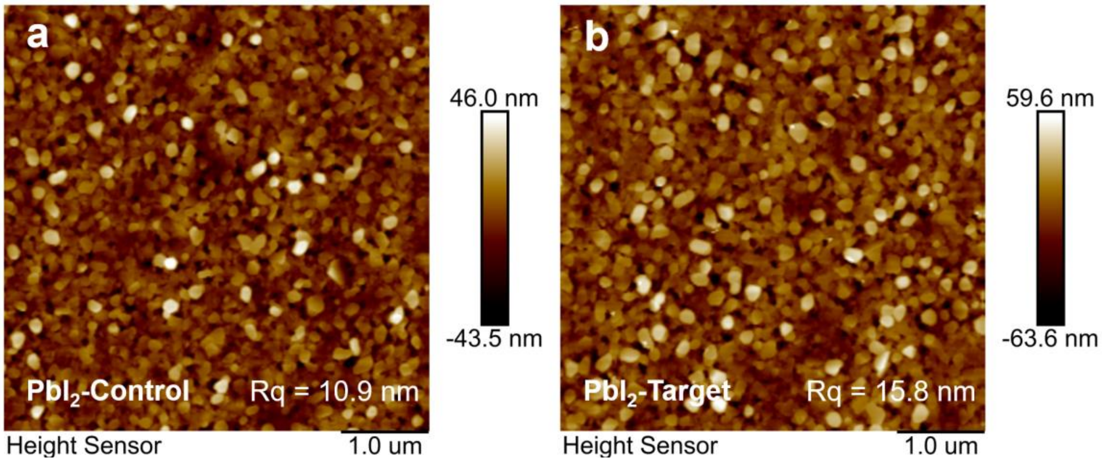

Figure S7. AFM images of the a) PbI_2-Control and b) PbI_2-Target annealed films deposited on ITO/SnO_2 substrates.

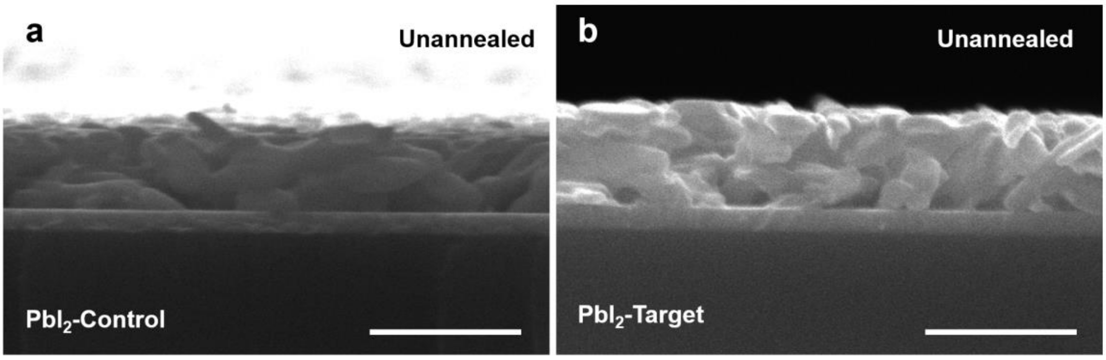

Figure S8. Cross-sectional SEM images of the a) PbI_2-Control and b) PbI_2-Target unannealed films deposited on ITO/SnO_2 substrates. The scale bars represent 1μm.

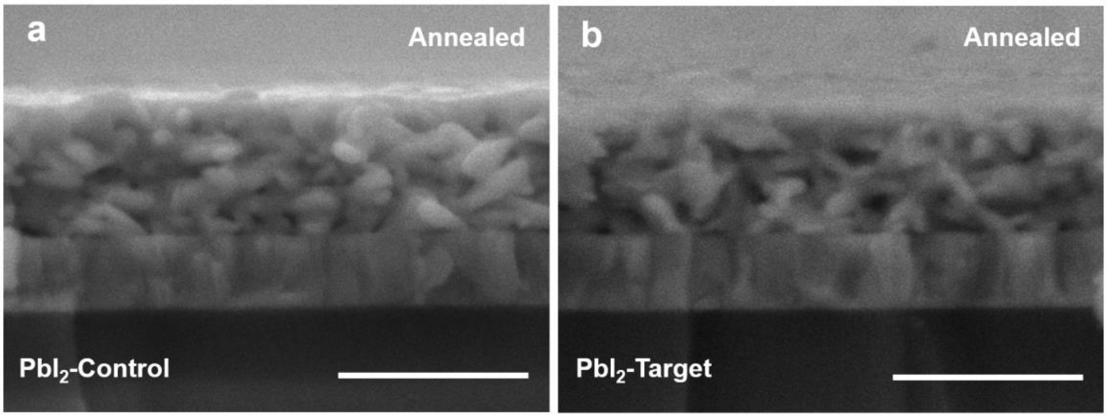

Figure S9. Cross-sectional SEM images of the a) PbI_2-Control and b) PbI_2-Target annealed films deposited on ITO/SnO_2 substrates. The scale bars represent 500 nm.

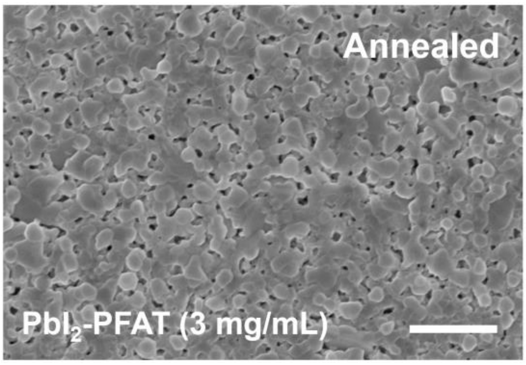

Figure S10. Top-view SEM image of a PbI_2-PFAT (3 mg/mL) annealed film deposited on an ITO/SnO_2 substrate. The scale bar represents 1µm.

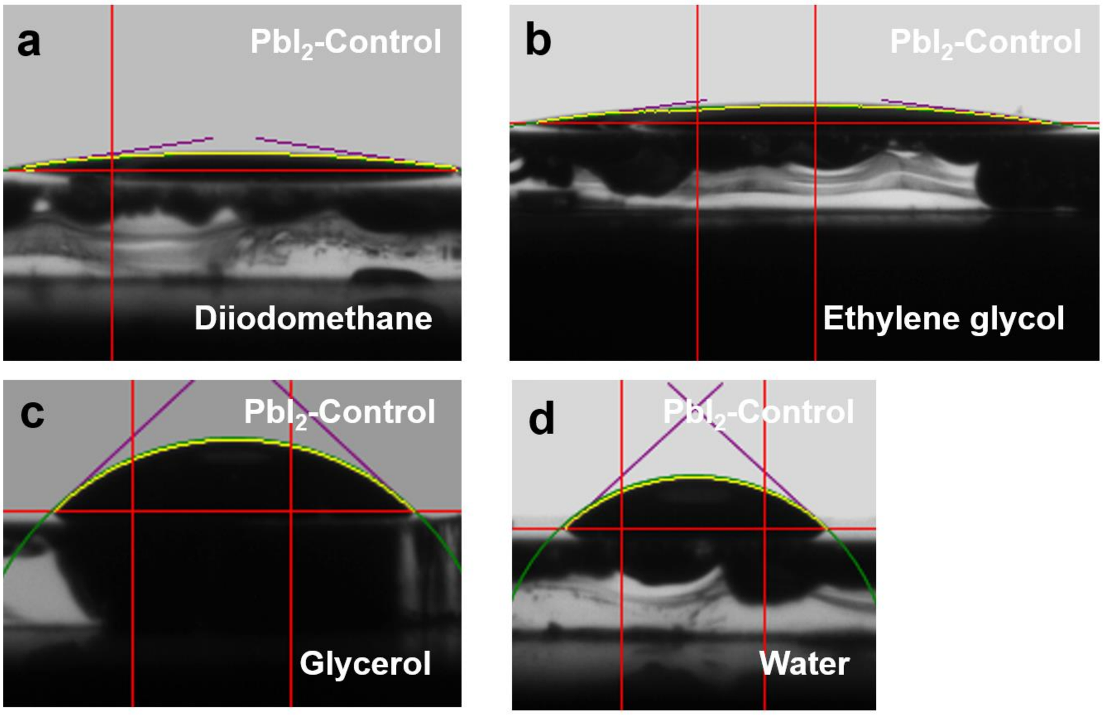

Figure S11. Contact angles of the PbI_2-Control films with a) diiodomethane, b) ethylene glycol, c) glycerol, and d) water solution droplets.

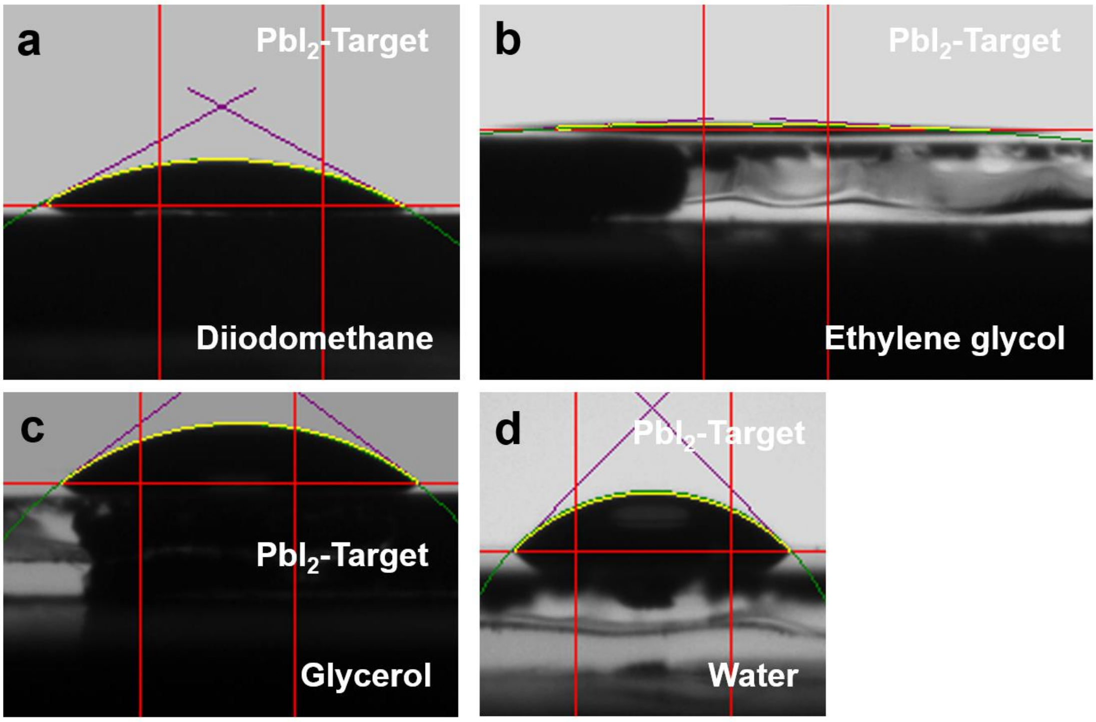

Figure S12. Contact angles of the PbI_2-Target films with a) diiodomethane, b) ethylene glycol, c) glycerol, and d) water solution droplets.

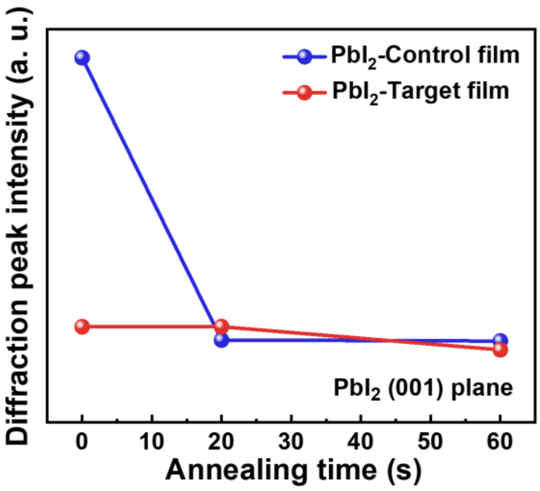

Figure S13. Evolution of diffraction peak intensity for (001) planes of different PbI_2 films with various annealing times.

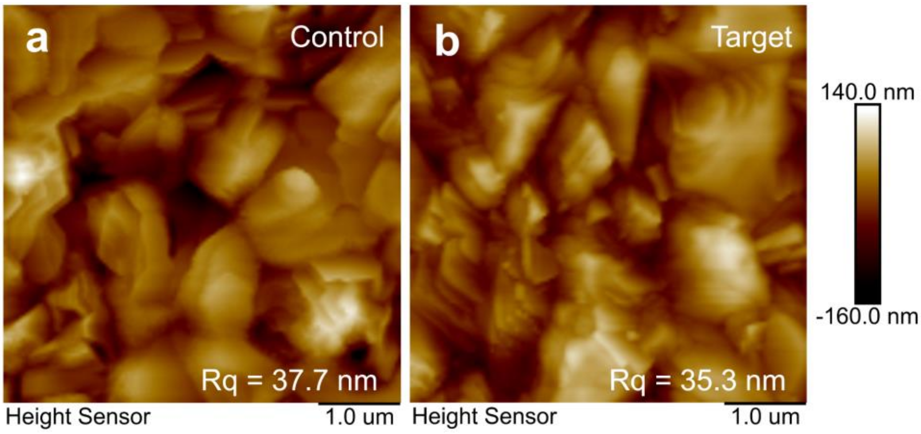

Figure S14. AFM images of the perovskite films a) without and b) with PFAT incorporation.

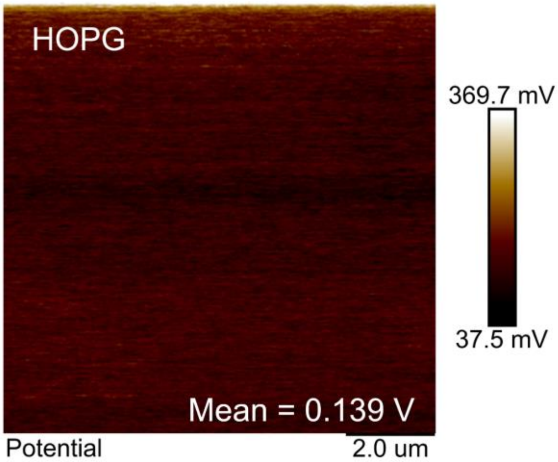

Figure S15. KPFM image of a highly oriented pyrolytic graphite (HOPG) as a standard sample.

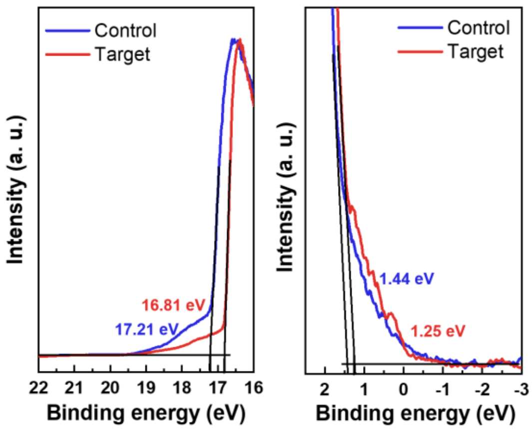

Figure S16. UPS spectra in the secondary electron cut-off regions (left) and valence band (VB) regions (right) of the control and target perovskite films. The laser energy source was He I (21.22 eV) for excitation.

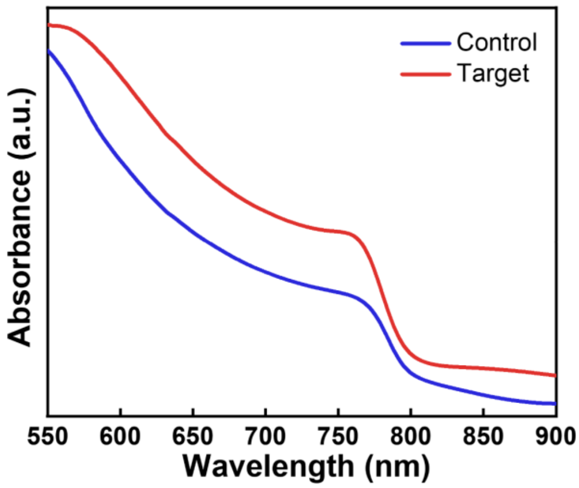

Figure S17. UV-vis absorbance spectra of the control and target perovskite films deposited on glass substrates.

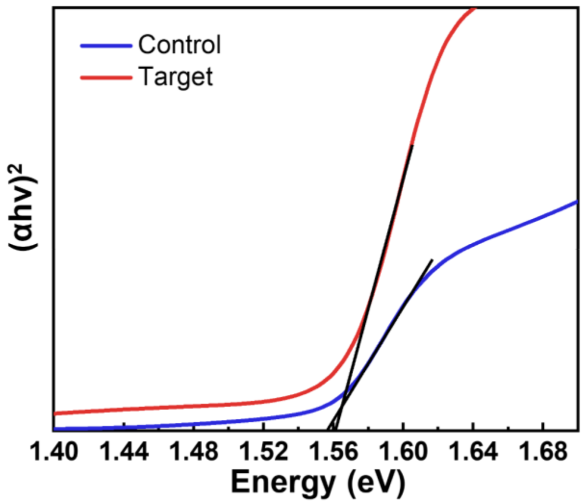

Figure S18. Tauc plots and measured bandgaps of the control and target perovskite films.

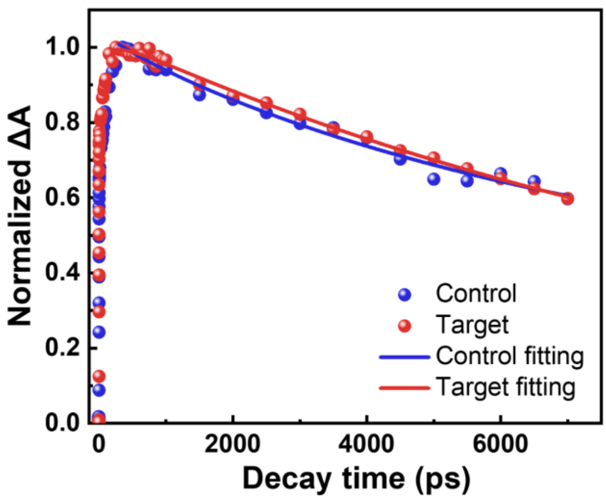

Figure S19. Normalized bleaching kinetics for different perovskite films.

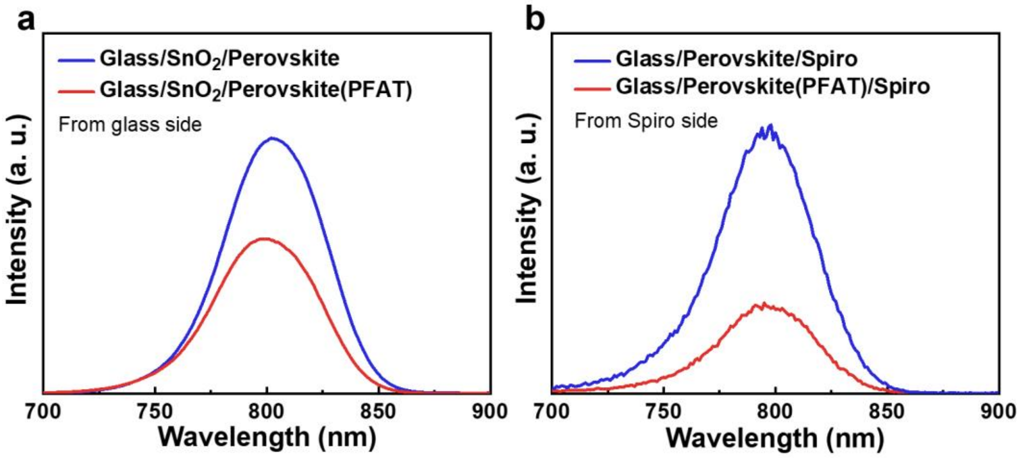

Figure S20. PL spectra of different perovskite films in the a) glass/SnO_2/perovskite and b) glass/perovskite/spiro-OMeTAD configurations.

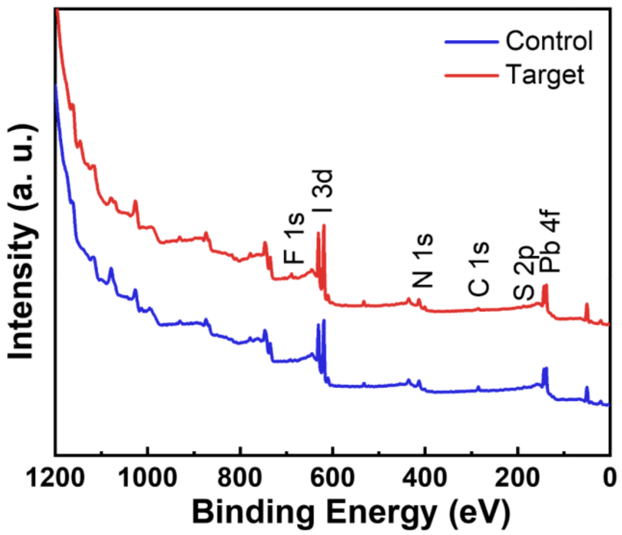

Figure S21. XPS full spectra of different perovskite films.

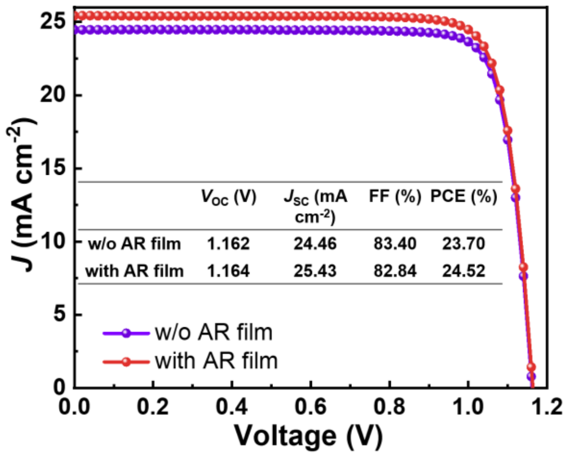

Figure S22. Comparison of photovoltaic parameters of the best-performing target device measured with reverse-scan without (w/o) and with a PDMS antireflective (AR) film.

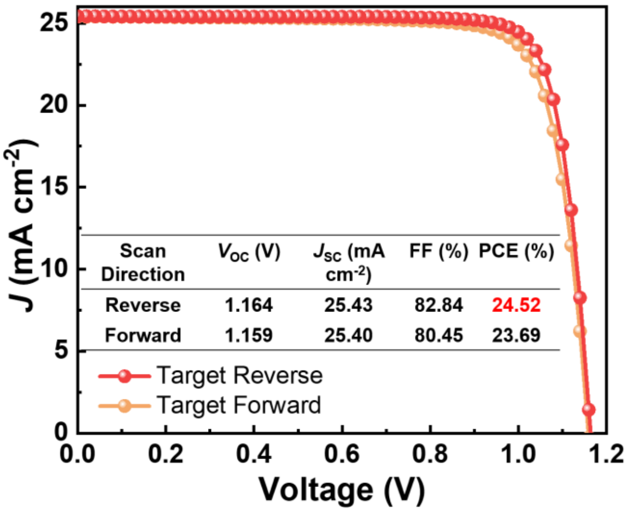

Figure S23. Reverse and forward-scanned *J*-*V* curves of the best-performing target device with a PDMS antireflective film.

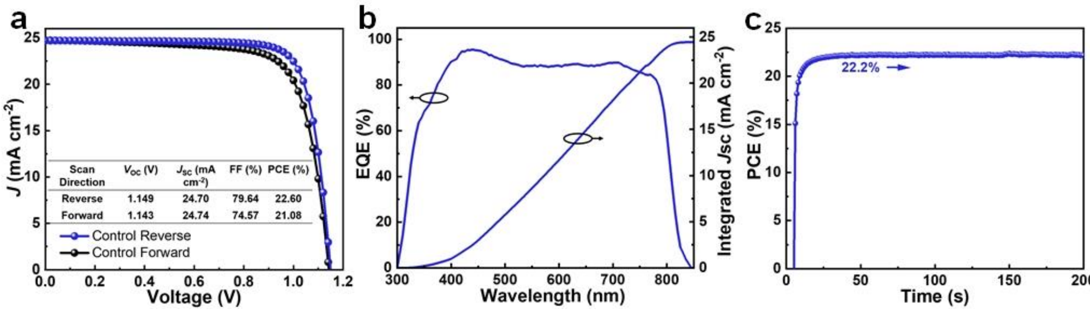

Figure S24. a) Reverse and forward-scanned *J*-*V* curves of the best-performing control device. b) EQE spectrum and integrated curve of the best-performing control cell. The integrated J_{SC} is 24.46 mA/cm^2. c) SPO test of the best-performing control device measured at a constant bias voltage of 0.94 V within 200 s. The steady-state PCE is ~22.2%.

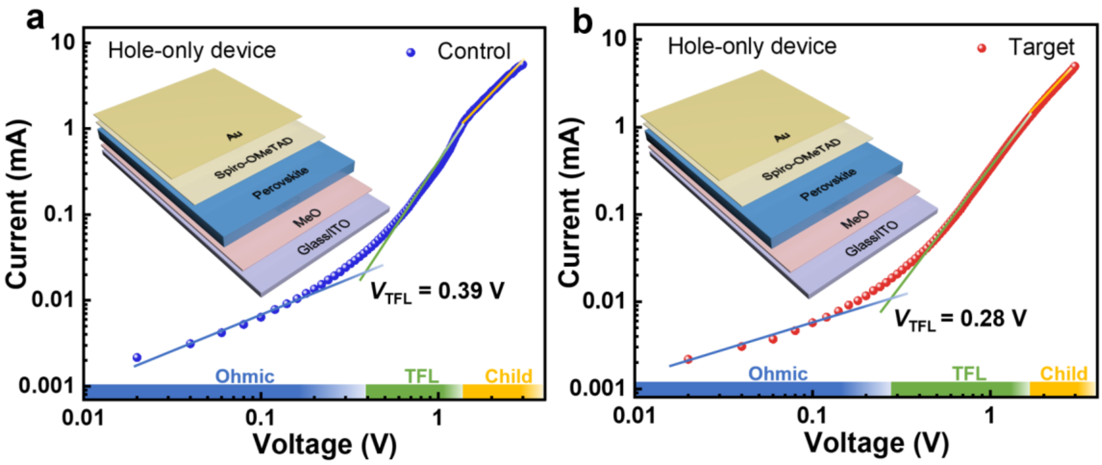

Figure S25. SCLC measurements for the hole-only a) control and b) target devices.

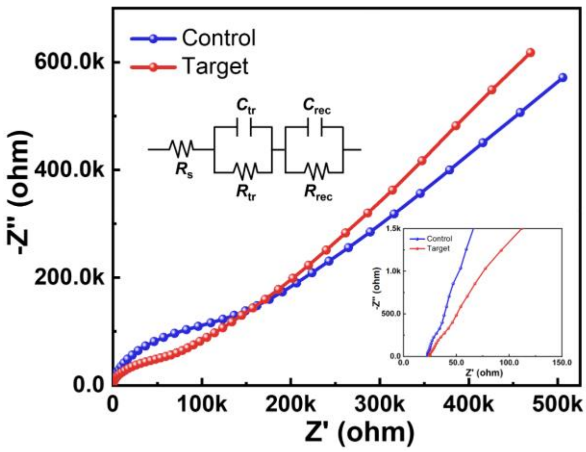

Figure S26. Nyquist plots of the control and target PSCs.

Table S1. Surface tension and contact angles between the standard liquids and the PbI_2 films without or with PFAT.

Liquid (L)	**Surface Tension (mN/m)**			**Contact angle θ (°)**	**x**	**y**	**m**	**c**
	Total σ	Dispersive σ_L^d	Polar σ_L^p					
PbI_2-Control film								
Diiodomethane	50.8	50.8	0	8.64	0	7.088	4.215	6.488
Ethylene glycol	48	29	19	7.649	0.81	8.874		
Glycerol	63.3	20.22	43.08	43.206	1.46	12.170		
Water	72.3	18.7	53.6	42.5	1.69	14.520		
PbI_2-Target film								
Diiodomethane	50.8	50.8	0	28.59	0	6.693	4.441	6.215
Ethylene glycol	48	29	19	3.298	0.81	8.905		
Glycerol	63.3	20.22	43.08	37.073	1.46	12.656		
Water	72.3	18.7	53.6	45.687	1.69	14.203		

Table S2. The fitted data of time-resolved TA spectra for different perovskite films.

Sample	A_1	τ_1 [ps]	A_2	τ_2 [ps]
Control	2.56E-2	697.2	6.85E-1	7613.3
Target	-5.64E-2	259.6	9.39E-1	11293.4

Table S3. TRPL lifetime parameters of the control and target perovskite films fitted by a bi-exponential decay function of $F(t) = A_1 \exp(-t/\tau_1) + A_2 \exp(-t/\tau_2) + \gamma_0$.

Sample	A_1 [%]	τ_1 [ns]	A_2 [%]	τ_2 [ns]	τ_{ave} [ns]
Control	5.26	213.23	94.74	1202.96	966.76
Target	4.34	181.74	95.66	2357.98	1551.57

Note S1. Calculation of the total surface tension (σ) of the PbI_2-Control and PbI_2-Target films.

The Owens-Wendt-Rabel-Kaelble (OWRK) model:

$$\frac{\sigma_L(1+\cos\theta)}{2\sqrt{\sigma_L^d}} = \sqrt{\sigma^p}\sqrt{\frac{\sigma_L^p}{\sigma_L^d}} + \sqrt{\sigma^d}$$

therein $y = \frac{\sigma_L(1+\cos\theta)}{2\sqrt{\sigma_L^d}}$, $x = \sqrt{\frac{\sigma_L^p}{\sigma_L^d}}$, the slope $m = \sqrt{\sigma^p}$, and the intercept $c = \sqrt{\sigma^d}$. By fitting the line $y = m * x + c$, we obtain $\sqrt{\sigma^p}$ and $\sqrt{\sigma^d}$, then the total surface tension $\sigma = \sigma^p + \sigma^d$.

Note S2. Estimation of Fermi energy levels from KPFM data.

The data obtained from KPFM measurements is contact potential difference (CPD, i.e., the mean value here). When DC voltage (V_{dc}) is applied to a sample, the relationship between the measured CPD and the work function (Φ) of the sample is $V_{CPD} = (\Phi_{sample} - \Phi_{tip})/e$. From Figure 2g, h and S15, we can list the following equations:

$$V_{CPD\text{-}HOPG} = (\Phi_{HOPG} - \Phi_{tip}) / e = 0.139 \text{ V},$$

$$V_{CPD\text{-}Control} = (\Phi_{Control} - \Phi_{tip}) / e = -0.367 \text{ V},$$

$$V_{CPD\text{-}Target} = (\Phi_{Target} - \Phi_{tip}) / e = -0.145 \text{ V},$$

then we obtain $\Phi_{Control} - \Phi_{HOPG} = -0.506$ eV, and $\Phi_{Target} - \Phi_{HOPG} = -0.284$ eV. Since $\Phi_{HOPG} = 4.5$ eV, $\Phi_{Control} = 3.994$ eV and $\Phi_{Target} = 4.216$ eV can be calculated.